

# Electronic Quenching of OH A $^2\Sigma^+$ Induced by Collisions with Kr Atoms

Julia H. Lehman,<sup>a</sup> Marsha I. Lester,<sup>\*,a</sup> Jacek Kłos,<sup>b</sup> Millard H. Alexander,<sup>b,c</sup> Paul J. Dagdigian,<sup>d</sup>  
Diego Herráez-Aguilar,<sup>e</sup> F. Javier Aoiz,<sup>e</sup> Mark Brouard,<sup>f</sup> Helen Chadwick,<sup>f</sup> Tom Perkins,<sup>f</sup> and  
Scott A. Seamons<sup>f</sup>

<sup>a</sup> Department of Chemistry, University of Pennsylvania, Philadelphia, PA 19104-6323 USA

<sup>b</sup> Department of Chemistry and Biochemistry, <sup>c</sup> Institute for Physical Science and Technology,  
University of Maryland, College Park, MD 20742-2021 USA

<sup>d</sup> Department of Chemistry, The Johns Hopkins University, Baltimore, MD 21218-2685 USA

<sup>e</sup> Departamento de Química Física, Facultad de Química, Universidad Complutense, Madrid,  
28040 Spain

<sup>f</sup> The Department of Chemistry, University of Oxford, The Physical and Theoretical Chemistry  
Laboratory, South Parks Road, Oxford, OX1 3QZ, United Kingdom

---

\* Corresponding author email: [milester@sas.upenn.edu](mailto:milester@sas.upenn.edu)

## ABSTRACT

Electronic quenching of OH  $A^2\Sigma^+$  by Kr is investigated through experimental studies of the collision cross sections and the OH  $X^2\Pi$  product distribution. The quenching cross sections decrease with increasing rotational excitation in the excited OH  $A^2\Sigma^+$  electronic state. The OH  $X^2\Pi$  products of quenching exhibit a significant degree of rotational excitation, but minimal vibrational excitation. Complementary theoretical studies of the OH ( $A^2\Sigma^+$ ,  $X^2\Pi$ ) + Kr potential energy surfaces (PES's), nonadiabatic coupling, and quasi-classical trajectory calculations are carried out to elucidate the quenching dynamics. Accurate PES's for the two lowest diabatic states of  $A'$  symmetry are computed along with the angularly dependent coupling between them. Coupling in near linear HO–Kr configurations provides the mechanism for the observed electronic quenching. A deep attractive well on the OH  $A^2\Sigma^+$  – Kr PES facilitates access to this region of strong coupling. Surface-hopping quasi-classical trajectory calculations yield quenching cross sections and OH  $X^2\Pi$  product rotational distribution in good accord with experimental observations.

**Keywords:** nonadiabatic dynamics, quenching cross section, conical intersection, quantum state distribution, hydroxyl radical

## INTRODUCTION

The hydroxyl radical is an important species in atmospheric and combustion environments, often detected using laser-induced fluorescence (LIF) on the OH  $A^2\Sigma^+ - X^2\Pi$  band system.<sup>1</sup> However, extensive kinetics studies have shown that these radicals are efficiently removed from the excited  $A^2\Sigma^+$  state via collisions with molecular or atomic partners, resulting in dramatically reduced fluorescence lifetimes and quantum yields. Kinetic studies have been carried out over a variety of temperatures and initial OH  $A^2\Sigma^+$  rotational level, showing that rates decrease with increasing temperature and OH  $A^2\Sigma^+$  rotational excitation.<sup>2-5</sup> A recent example of such studies is the quenching cross section measurements for various spin-rotation levels of OH  $A^2\Sigma^+$  for Kr by Chadwick *et al.*<sup>6</sup> These trends are indicative of a quenching mechanism controlled by an attractive interaction on the excited state potential energy surface (PES) that depends on OH orientation.<sup>2-5</sup>

Molecular partners, such as H<sub>2</sub> ( $\sim 8 \text{ \AA}^2$ ) and N<sub>2</sub> ( $\sim 5 \text{ \AA}^2$ ), have large quenching cross sections at room temperature. On the other hand, rare gas colliders typically have negligibly small quenching cross sections ( $\sigma_Q \sim 0.004 \text{ \AA}^2$  and  $0.047 \text{ \AA}^2$  for He and Ar, respectively).<sup>7-9</sup> In contrast, the heavier rare gases, starting with Kr ( $\sigma_Q \sim 8 \text{ \AA}^2$  at 300 K),<sup>6</sup> have quenching cross sections very similar in magnitude to those of the molecular partners.<sup>10</sup> As we show in this study, the PES's emanating from the OH  $A^2\Sigma^+$  and  $X^2\Pi$  states cross at energies thermally accessible from the excited state.

In order to gain further insight into the quenching mechanism, recent experimental studies in one of our laboratories (University of Pennsylvania), and others,<sup>11,12</sup> have focused on the outcomes of the quenching event. Characteristics of the reactive (forming new products) and/or nonreactive (returning OH to its ground  $X^2\Pi$  state) events have been studied for several

quenching partners ( $\text{H}_2$ ,  $\text{D}_2$ ,  $\text{N}_2$ ,  $\text{CO}$ ,  $\text{CO}_2$ ,  $\text{O}_2$ ).<sup>11,13-20</sup> Branching fractions have also been determined.<sup>14-20</sup> The importance of the nonreactive  $\text{OH } X^2\Pi$  ( $v''=0-2$ ) pathways varies significantly with collision partner, ranging, for example, from 12% for  $\text{H}_2$  to 88% for  $\text{N}_2$ . The focus of the Oxford laboratory has been on the fate of the electronically excited OH that survives the quenching process and remains electronically excited after the collision.

On the other hand, the characteristics of the  $\text{OH } X^2\Pi$  product state distributions following nonreactive quenching of  $\text{OH } A^2\Sigma^+$ , in which 4.06 eV of electronic energy is released to products, are quite similar for most collision partners. The  $\text{OH } X^2\Pi$  product is released with a high degree of rotational but little vibrational excitation. In the  $\text{OH} + \text{H}_2$  system, the rotational distribution is peaked about  $N'' = 15$  with an average rotational energy  $\langle E_{\text{rot}} \rangle = 4480 \text{ cm}^{-1}$  in  $v''=0$ .  $\text{OH } X^2\Pi$  is produced predominately in  $v''=0$  (75%) with less products found in  $v''=1$  (20%) and  $v''=2$  (5%). Collisional quenching with  $\text{N}_2$  results in an even higher degree of rotation ( $\langle E_{\text{rot}} \rangle = 6540 \text{ cm}^{-1}$  in  $v''=0$ ), with less energy going into OH vibration (97% of the products are found in  $v''=0$ ). Both collision partners also show a preference for populating the  $\Pi(A')$   $\Lambda$ -doublet component, where the unpaired electron of  $\text{OH } X^2\Pi$  lies in a  $p\pi$  orbital within the plane of nuclear rotation.<sup>21</sup> For collisions of  $\text{OH } A^2\Sigma^+$  with Kr, only nonreactive quenching can occur. Based on the  $\text{OH } X^2\Pi$  product state distribution seen in other systems, we might anticipate similar trends following quenching by Kr.

The pairing of experiment with theory has been essential for understanding the quenching process. For this reason, the  $\text{OH} + \text{H}_2$  system has emerged as a benchmark for elucidating the quenching mechanism. Theoretical work has identified regions of conical intersection accessible from  $\text{OH } A^2\Sigma^+ + \text{H}_2$  when the oxygen side of OH points toward  $\text{H}_2$ .<sup>13,22-25</sup> These regions of

strong nonadiabatic coupling allow population to be funneled from the excited state surface to OH  $X^2\Pi$  + H<sub>2</sub> or H<sub>2</sub>O + H products. Interestingly, when the hydrogen side of OH  $A^2\Sigma^+$  points toward H<sub>2</sub>, there is an attractive electrostatic interaction but no pathway leading to quenching.<sup>13,23,26</sup>

Characteristics of the conical intersection and topography of the PES have been used to explain, at least qualitatively, the significant rotational and minimal vibrational excitation of the OH  $X^2\Pi$  products.<sup>13,22,25</sup> Recently, classical trajectory<sup>19,27-29</sup> and quantum scattering calculations<sup>30,31</sup> for the OH  $A^2\Sigma^+$  + H<sub>2</sub> system yielded OH  $X^2\Pi$  product distributions and branching fractions similar to those measured experimentally. In the OH + N<sub>2</sub> system, *ab initio* calculations identified an energetically accessible conical intersection coupling the ground and electronically excited state surfaces, again when the oxygen side of OH  $A^2\Sigma^+$  points toward the N<sub>2</sub> partner.<sup>17</sup> In the OH–N<sub>2</sub> configuration, there is also an attractive intermolecular interaction but no pathway for quenching.<sup>23</sup> The forces in the region of conical intersection indicate a propensity toward nonreactive products with a large degree of OH rotation and comparatively less OH vibration with N<sub>2</sub> than predicted for H<sub>2</sub>, which is consistent with experimental results.<sup>17</sup>

The majority of previous experimental and theoretical studies for the OH ( $X^2\Pi$ ,  $A^2\Sigma^+$ ) + Kr system have been focused on the OH–Kr van der Waals complex formed when the H-side of OH  $X^2\Pi$  interacts with Kr and its subsequent electronic excitation.<sup>32-35</sup> High-resolution electronic spectroscopy studies by Miller and coworkers enabled analysis of several vibronic bands of OH–Kr on the  $A^2\Sigma^+ - X^2\Pi$  transition.<sup>32,33</sup> These authors derived rotational constants and bond lengths for the ground state and several vibronic levels in the excited electronic state. In addition, they characterized intermolecular stretch progressions with and without bend excitation in the excited electronic state. The spectroscopic data were then utilized to develop an

empirical PES for OH  $A^2\Sigma^+ + \text{Kr}$ , which was reliable primarily in the  $\theta \leq 60^\circ$  region about the linear OH–Kr (Jacobi angle  $\theta = 0^\circ$ ) minimum energy configuration. This PES predicts a well depth of  $D_e \sim 2420 \text{ cm}^{-1}$  at  $R_e = 5.24 a_0$ . A second well in the linear HO–Kr configuration was estimated to have a well depth of  $1900 \text{ cm}^{-1}$  at a much shorter intermolecular distance of  $4.16 a_0$ .

More recent *ab initio* RCCSD(T) calculations mapped out the electronically excited OH  $A^2\Sigma^+ + \text{Kr}$  PES for a fixed OH bond length.<sup>6</sup> This study revealed a significantly deeper potential well in the linear HO–Kr ( $\theta = 180^\circ$ ) configuration than the prior empirical PES with a substantially larger well depth of  $D_e \sim 6079 \text{ cm}^{-1}$  at  $R_e \sim 4.16 a_0$ . The HO–Kr minimum is separated from the linear OH–Kr configuration by a large barrier (greater than  $1850 \text{ cm}^{-1}$ ). The properties of the OH–Kr well and its energy level structure were in reasonable agreement with the prior work by Miller and coworkers, although some vibrational level reassignments were suggested. The study of Chadwick *et al.*<sup>6</sup> also included new experimental measurements of OH  $A^2\Sigma^+ - \text{Kr}$  rotationally-inelastic scattering cross sections using Zeeman quantum beat spectroscopy. Both quantum mechanical and quasi-classical trajectory scattering calculations were performed on the new OH  $A^2\Sigma^+ + \text{Kr}$  PES, yielding cross sections, which were in good agreement with experiment.<sup>6</sup>

In this paper, we report the nascent OH  $X^2\Pi$  product state distribution, including vibrational, rotational, and fine-structure propensities, as well as the cross sections for the quenching of OH  $A^2\Sigma^+$  by Kr. Our measurements probe the regions of the OH  $A^2\Sigma^+ + \text{Kr}$  excited state PES that allow for nonadiabatic coupling and efficient population transfer from the excited state to the OH  $X^2\Pi + \text{Kr}$  ground state surface. Complementary theoretical calculations show that the nonadiabatic coupling occurs in the HO–Kr well region, which has heretofore not been probed experimentally. The observed product distributions are a measure of the forces on

the OH radical as it passes through the strong nonadiabatic coupling region and subsequently separates from Kr on the ground state surface.

## EXPERIMENTAL METHODS

Two types of experiments were performed. The first, performed under jet expansion conditions (average collision energy of  $\sim 0.025$  eV) at the University of Pennsylvania, were used to determine lifetime and OH  $X^2\Pi$  population data. The second set, performed under thermal conditions at 300 K at the University of Oxford, were used to determine thermally averaged collisional quenching cross-sections. Since collisional quenching of OH  $A^2\Sigma^+$  by many partners is known to be temperature-dependent, the two experiments cannot be compared quantitatively.

**Lifetime and Population Measurements.** The experimental methods for investigating the outcomes following collisional quenching of OH  $A^2\Sigma^+$  by Kr are similar to those used previously at the University of Pennsylvania for other quenching partners.<sup>13,14,16,17,19</sup> Briefly, OH  $X^2\Pi$  radicals are generated in the throat of a pulsed supersonic jet expansion by photolyzing nitric acid (98% fuming) at 193 nm. The nitric acid vapor is entrained in a 20% Kr/He gas mixture with a backing pressure of 80 psi. In the collision region of the expansion at a distance of  $x/D = 5$  in nozzle diameters  $D$ , the OH radicals are excited on the  $P_1(1)$  line of the  $A^2\Sigma^+ - X^2\Pi(0,0)$  transition with the UV pump laser operating at 308 nm. The pump laser induced fluorescence (LIF) is collected with a photomultiplier tube (PMT, ET Enterprises 9813Q) using a 308 nm bandpass filter. After a 100 ns delay, a spatially overlapped and counter propagating UV laser intersects the expansion and probes the quenched OH  $X^2\Pi$  products by means of various OH  $A-X$  transitions with vibrational ( $v''$ ), rotational ( $N''$ ), and fine-structure resolution. Probe LIF signals are collected using the same PMT but with different bandpass filters. The probe

laser excitation and fluorescence collection schemes are the same as used in prior experiments with N<sub>2</sub> as a collision partner.<sup>17</sup>

The LIF signals are processed with a digital storage oscilloscope (LeCroy WaveRunner 6050A) and transferred to a laboratory computer for further analysis. The waveform traces are fit to single exponential decays to determine fluorescence lifetimes and integrated over a fixed gate to obtain intensities. The probe LIF intensities, recorded under saturated LIF conditions, are scaled relative to a reference line and converted to relative OH X <sup>2</sup>Π populations using the same analysis procedure that has been described previously.<sup>13,14,16,17,19</sup> The analysis procedure accounts for the lifetime and fluorescence quantum yield ( $\Phi_f$ ) of the emitting state as well as the filter transmission function.

An active background subtraction scheme,<sup>13,14,16,17,19</sup> is used in data collection. Briefly, the pump laser (5 Hz) is operated at half the repetition rate of the probe laser (10 Hz). The background signal arising from the probe laser only is subtracted from the combined pump and probe laser-induced signal. This scheme enables one to distinguish between the desired signal arising from the combination of pump and probe lasers, and background signals originating from the probe laser only.

**Thermally averaged electronic quenching cross-sections.** Absolute, thermally averaged cross-sections for electronic quenching of OH A <sup>2</sup>Σ<sup>+</sup> by Kr at 300 K were measured at the University of Oxford. The methods used are the same as described in previous studies<sup>6</sup> and so are summarized here only briefly.

OH X <sup>2</sup>Π is generated by the photolysis of hydrogen peroxide or nitric acid at 193 nm, and is excited to the A <sup>2</sup>Σ<sup>+</sup> state on the (0,0) band with a pulsed dye laser after a delay of around 10 μs to allow the radicals to thermalize translationally. A photoelastic modulator (PEM) is used



to switch the laser polarization direction either parallel or perpendicular to the detection axis on alternate shots. The resulting fluorescence from OH  $A^2\Sigma^+$  passes through a linear polarizer and is detected by a photomultiplier tube.

The fluorescence traces from parallel ( $I_{\parallel}$ ) and perpendicular ( $I_{\perp}$ ) laser polarization directions with respect to the detection axis are fitted using  $I_{\parallel} + 2I_{\perp}$ , which is sensitive only to the decay in population, and independent of the decay in polarization. The data are fitted to a single exponential

$$I = A e^{-(k_f + k_Q[\text{Kr}])t} \quad (1)$$

where  $k_f$  is the inverse of the fluorescence lifetime and  $k_Q$  is the quenching rate constant. By measuring decays over a range of Kr pressures in the range ~100 mTorr to ~600 mTorr,  $k_Q$  can be determined and converted into a thermal averaged quenching cross-section *via*  $\sigma_Q = k_Q(T)/\langle v_{\text{rel}} \rangle$ . Errors are taken as one standard deviation for comparison with the literature.<sup>5</sup>

In these unresolved measurements, rotational energy transfer (RET) does not directly contribute to the decay rate of the OH(A) emission. However, significant rotational energy transfer between rotational levels of OH(A) would scramble the initial state selectivity of the electronic quenching measurements. For this reason, only the first ~100 ns of the fluorescence decay was fitted to ensure that the measured electronic quenching rate constants were specific to a single  $N$  level. Detailed simulations and fits were performed, as described in Ref. 36, to verify that this procedure yielded the correct initial state selected electronic quenching rate constants within the quoted errors in the measurements.

## EXPERIMENTAL RESULTS

**OH A  $^2\Sigma^+$  Lifetimes.** The OH radicals prepared in the lowest rovibrational level ( $v=0$ ,  $N=0$ ) of the excited A  $^2\Sigma^+$  electronic state have a fluorescence lifetime of 400(15) ns in the collisional region of the supersonic expansion, which is significantly shorter than the radiative lifetime of  $\sim 700$  ns. Collisions with Kr in the 20% Kr/He carrier gas mixture are relatively efficient in quenching the OH A  $^2\Sigma^+$  ( $v=0$ ,  $N=0$ ); pure He carrier gas does not quench the fluorescence. Using a 20% N<sub>2</sub>/He carrier gas mixture at 80 psi under similar experimental conditions, the fluorescence lifetime is approximately 320 ns ( $k_{\text{tot}}^{-1}$ ). The fluorescence lifetimes are measured for each of the OH A  $^2\Sigma^+$  ( $v=0, 1, N$ ) levels accessed by the probe laser, shown in Fig. 1 with values at each  $N$  averaged over spin-rotation components. These data are used in the analysis of OH X  $^2\Pi$  populations. The experimentally measured total rates ( $k_{\text{tot}}$ ) are the sum of the collisional ( $k_{\text{coll}}$ ), radiative ( $k_{\text{rad}}$ ), and electronic predissociation ( $k_{\text{PD}}$ ) rates at each  $N$ . The radiative and electronic predissociation rates for OH A  $^2\Sigma^+$  are tabulated in LIFBASE.<sup>37</sup> The pseudo-first-order collisional rates,  $k_{\text{coll}}$ , are readily extracted and are plotted in Fig. 1.

In OH A  $^2\Sigma^+$  ( $v=0$ ), the pseudo-first-order collisional rate is due solely to collisional quenching. The rate is largest for  $N=0$  and smaller for the high  $N$  levels examined in this work, remaining fairly constant from  $N=18$ -22, but then increasing slightly at high  $N$ ; the latter effect is similar, but to a lesser extent, than that seen previously in collisions with N<sub>2</sub>.<sup>17</sup> These highest  $N$  levels are above the energetic threshold to  $v=1$ , possibly indicating a rotational ( $v=0$ , high  $N$ ) to vibrational ( $v=1$ , low  $N$ ) energy transfer process. In OH A  $^2\Sigma^+$  ( $v=1$ ), the collisional rate is the sum of the collisional quenching and vibrational energy transfer rates, which cannot be decoupled in this experiment. The collisional rate decreases with increasing  $N$ . In the present experiments with Kr, the radiative rate at low  $N$  is larger than the collisional rate.

**OH A  $^2\Sigma^+$  Electronic Quenching Cross-Sections.** Absolute, thermally averaged electronic quenching cross-sections at 300 K for OH A  $^2\Sigma^+$  by Kr are presented in Fig. 2, which is split into two panels for quenching from  $F_1$  ( $j = N+S$ ) and  $F_2$  ( $j = N-S$ ) spin-rotation levels of OH A  $^2\Sigma^+$ . Figure 2 presents a much more extensive data set than that reported in our previous publication.<sup>6</sup> The thermally averaged cross-sections are compared to the results of Hemming *et al.*<sup>5</sup> (note that the spin-rotation level employed was not specified in that work). Agreement with the literature is seen to be excellent and supports the smooth downward trend in  $\sigma_Q$  with  $N$ , falling to zero around  $N = 10$ . As the OH(A) radical rotates faster, fewer collisions are able to sample the conical intersection region in the HO(A)–Kr well, and as a consequence are unable to undergo electronic quenching. Only a very small difference is observed between the electronic quenching cross-sections for the  $F_1$  and  $F_2$  spin-rotation levels.

**OH X  $^2\Pi$  Product State Distribution.** Relative populations have been measured for over 40 distinct OH X  $^2\Pi$  product quantum states. In some cases, individual OH X  $^2\Pi$  levels could not be probed due to spectral congestion, the rapid onset of predissociation at high  $N$  especially in  $v''=1$ , or a large OH X  $^2\Pi$  background at low  $N''$  ( $v''=0$ ) preventing acceptable signal-to-noise ratios during the active background subtraction procedure. The population distribution is shown in Figs. 3 and 4, plotted as a function of OH X  $^2\Pi$  internal energy and then again as rotational quantum number.

To aid in analysis of the population distribution, an arbitrary functional form was fit to the distribution after scaling  $v''=1$  to  $v''=0$ . A sum of two Fisher-Tippett functions was used here in order to capture the shape of the distribution.<sup>38</sup> The  $v''=0$  and  $v''=1$  distributions have similar shapes, exhibiting a peak around 9 quanta of rotation, a slight dip in population and then a second peak around 17 quanta of rotation. The distribution drops off at high and low  $N''$ . The

population in specific product states were compared between  $v''=0$  and  $v''=1$ . This led to a ratio of  $\sim 7$  times more population in  $v''=0$  than  $v''=1$ .

In  $v''=0$ , all four spin-orbit ( $F_1$  and  $F_2$ ) and  $\Lambda$ -doublet ( $\Pi(A')$  and  $\Pi(A'')$ ) states were probed for  $N''=11-16$ . For a given  $\Lambda$ -doublet component, populations in equivalent (same  $N''$ )  $F_1$  and  $F_2$  levels were found to be approximately the same within experimental uncertainty. The degree of electron alignment (DEA) is defined as  $[P_{\Pi(A')} - P_{\Pi(A'')}] / [P_{\Pi(A')} + P_{\Pi(A'')}]$ , which has limiting values of  $+1$  and  $-1$  associated with the unpaired electron in the  $p\pi$  orbital aligned in and out of the plane of molecular rotation, respectively. The DEA was found to be  $0.06(7)$ , indicating little to no  $\Lambda$ -doublet propensity. This was tested again at a shortened pump-probe time delay (40 ns) with the same result within experimental uncertainty.

A branching fraction measurement was carried out following analogous studies with other quenching partners.<sup>15-17,19</sup> The amount of initially prepared OH  $A^2\Sigma^+$  ( $v=0$ ,  $N=0$ ) was compared to four different OH  $X^2\Pi$  product levels, two in  $v''=0$  and two in  $v''=1$ . Approximately 1.1% of the quenched products are found in  $N''=13$  and 14 of  $v''=0$ , 0.12% in  $N''=13$  of  $v''=1$ , and 0.16% in  $N''=15$  of  $v''=1$ . To determine the total branching to OH  $X^2\Pi$  ( $v''=0, 1$ ) products, the fit to the data is used to estimate the population in unobserved quantum states. Assuming a DEA = 0.06 and equal population in  $F_1$  and  $F_2$  states, approximately 95(7)% of total quenched population can be identified in  $v''=0$  [83(7)%] and  $v''=1$  [12(1)%].

## THEORETICAL METHODS AND RESULTS

**Potential Energy Surfaces and Couplings.** The ground  $X^2\Pi$  and first excited  $A^2\Sigma^+$  states of the OH molecule differ in the filling of the non-bonding  $2p_\pi$  and bonding  $3\sigma$  orbital (formed from the bonding combination of the O  $2p_\pi$  and H  $1s$  orbitals). The electronic

configuration of the  $X$  state is  $2p_{\pi}^3 3\sigma^2$  while that of the  $A$  state is  $2p_{\pi}^4 3\sigma^1$ . The  $A$  state lies 4.06 eV above the ground state.

Approach of the spherically symmetric Kr atom lifts the degeneracy of the  $2p_{\pi}$  orbitals, splitting the  $\Pi$  state into a state which is symmetric ( $A'$ ) with respect to reflection in the plane of the three atoms (which we take to be the  $yz$  plane), with electronic configuration  $2p_{\pi x}^2 2p_{\pi y}^1 3\sigma^2$ , and a state which is antisymmetric ( $A''$ ), with electronic configuration  $2p_{\pi x}^1 2p_{\pi y}^2 3\sigma^2$ . We will label these states  $\Pi_{A'}$  and  $\Pi_{A''}$ , respectively. In non-linear geometries approach of the Kr can mix the  $A'$  component of the  $X^2\Pi$  state with the  $A^2\Sigma^+$  state, in which the electronic wavefunction has also  $A'$  reflection symmetry. We will label this second  $A'$  state as  $\Sigma_{A'}$ . This  $\Pi/\Sigma$  notation for the two diabatic states of  $A'$  reflection symmetry follows earlier work on electronic quenching by Alexander and Corey<sup>39</sup> and Dagdigian *et al.*<sup>40</sup> For illustration, we show contour plots of the OH  $\Sigma_{A'}$  (panel a) and  $\Pi_{A'}$  (panel b) molecular orbitals discussed above as the Kr atom approaches the relevant states of OH in Fig. 5. The  $\Pi_{A''}$  molecular orbital (not shown) is similar to the  $\Pi_{A'}$  orbital in panel b, but perpendicular to the triatomic plane.

As mentioned before, last year Chadwick *et al.* reported<sup>6</sup> calculations of the Kr–OH ( $A^2\Sigma^+$ ) PES that revealed a deep minimum for collinear Kr–OH approach. These authors characterized the single  $\Sigma_{A'}$  PES at the coupled-cluster [RCCSD(T)] level and calculated rovibrational bound levels and cross sections for rotational energy transfer (RET) within the  $A^2\Sigma^+$  state. The calculated RET cross-sections obtained on the single PES surface slightly overestimated the experimental results, which suggested the presence of a collisional quenching pathway, not included in the theoretical model. The *ab initio* PES of Chadwick *et al.*<sup>6</sup> was determined within a coupled-cluster method, which is single-reference in nature and cannot describe well the two PES's of  $A'$  symmetry in the region where they cross. Here, we show that

the crossing between  $\Pi_{A'}$  and  $\Sigma_{A'}$  Kr–OH PESs leads to significant non-radiative collisional quenching.

To determine the  $\Pi_{A'}$  and  $\Sigma_{A'}$  Kr–OH PESs, the coupling between these two diabatic states, and the PES for the single state of  $A''$  reflection symmetry ( $\Pi_{A''}$ ), we used the MOLPRO suite of *ab initio* codes. We maintained the OH distance to be that of isolated OH in the  $A$  state,  $r_e=1.0121$  Å.<sup>41</sup> We used an augmented correlation-consistent triple-zeta basis set, optimized for all-electron scalar relativistic calculations with Douglas–Kroll integrals (aug-cc-pvtz-DK).<sup>42</sup> Multi-configurational Hartree-Fock (MCSCF) calculations were done, followed by a multi-reference configuration-interaction calculations with inclusion of single and double excitations and, finally, the addition of the Davidson correction (MRCISD+Q) to reduce the error associated with lack of size consistency.

These calculations yield three adiabatic PES's, two of  $A'$  and one of  $A''$  reflection symmetry, which we label  $1A'$ ,  $2A'$ , and  $1A''$ . Making use of the quasi-diabatization capability in MOLPRO, we then transform, as defined in the next two equations, the  $1A'$  and  $2A'$  adiabatic states into the  $\Pi_{A'}$  and  $\Sigma_{A'}$  quasi-diabatic basis. The adiabatic and diabatic states of  $A'$  reflection symmetry are related by a  $2 \times 2$  orthogonal transformation, as follows:

$$\begin{bmatrix} V_{1A'} & 0 \\ 0 & V_{2A'} \end{bmatrix} = \mathbf{C} \begin{bmatrix} V_{\Pi_{A'}} & V_{\Sigma\Pi} \\ V_{\Sigma\Pi} & V_{\Sigma_{A'}} \end{bmatrix} \mathbf{C}^T \quad (2)$$

where

$$\mathbf{C} = \begin{bmatrix} \cos \gamma & \sin \gamma \\ -\sin \gamma & \cos \gamma \end{bmatrix} \quad (3)$$

Here, the mixing angle  $\gamma$  as well as the two diagonal and the off-diagonal diabatic PESs are a function of the three internal coordinates of the OH-Kr system. As expressed in Eqs. (2) and (3),

the two adiabatic states represent an orthogonal admixture of the electronic configuration of the A-state and the electronic configuration of the A' component of the X state.

In the quasi-diabatization the MCSCF orbitals are first rotated to maximize the overlap with a set of reference orbitals, taken here to be those for collinear KrOH at large Kr–O distance, where the A and X state are well separated in energy. The three diabatic PESs are then obtained by analysis of the CI coefficients in the basis of configurations built from the rotated orbitals. The third quasi-diabatic state,  $\Pi_{A''}$ , is unaffected by the adiabatic→quasi-diabatic transformation of the two A' states, and is identical to the  $1A''$  adiabatic state. At large OH–Kr distances, the two diabatic and adiabatic states of A' reflection symmetry become identical and correlate with the OH(X)+Kr and OH(A)+Kr asymptotes.

In the electronically adiabatic basis, the off-diagonal matrix elements of the derivative operator are responsible for the nonadiabatic coupling between the two states of A' symmetry. It is easy to show, from Eqs. (2) and (3), that this matrix element – the so-called nonadiabatic coupling matrix element (NACME) – is equal to the derivative of the mixing angle, namely

$$\langle 1A' | \frac{\partial}{\partial q} | 2A' \rangle = \frac{\partial \gamma}{\partial q} \quad (4)$$

where  $q$  designates any of the three Jacobi coordinates. Equivalently, we can use the gradient operator to define a nonadiabatic coupling vector

$$\langle 1A' | \vec{\nabla}_q | 2A' \rangle = \vec{\nabla}_q \gamma \quad (5)$$

The PES's were determined on a grid in Jacobi coordinates,  $R$  (ranging from 2.75 to 15 bohr) and  $\theta$  (ranging from 0° to 180° every 20° including 90°). To obtain interaction energies, we subtract the energy at a large separation between Kr and OH. The calculated interaction energies were not corrected for basis-set superposition error. Figure 6 shows radial cuts of the resultant

adiabatic and diagonal diabatic PESs of  $A'$  symmetry in near linear configurations. Figure 7 shows a surface plot of the two diabatic states, oriented to show clearly the small region of the crossing. This figure represents a 2-D extension of Fig. 6. Figure 8 displays a surface plot of the  $V_{\Sigma\Pi}$  PES, which is the off-diagonal coupling in the diabatic basis.

In linear geometry, the  $V_{\Sigma A'}$  PES is crossed by the repulsive wall of the  $V_{\Pi A'}$  PES at energies below the  $\text{Kr}+\text{OH}(A)$  asymptote, as shown in Fig. 6 for  $\theta = 170^\circ$ . It is the presence of the deep, close-in  $\text{Kr}-\text{OH}(A)$  minimum that permits collisions at thermal and modestly hyperthermal energies to access this crossing. In the other collinear geometry ( $\text{Kr}-\text{HO}$ ) a crossing occurs, but at much higher energy far above the  $\text{Kr}+\text{OH}(A)$  asymptote, as illustrated in Fig. 6 for  $\theta = 10^\circ$ . The conical intersections in the two linear geometries become avoided crossings in bent geometries, as shown in Fig. 6.

This mixing of the two diabatic states provides a mechanism for electronic quenching of the  $\text{OH } A$  state in collisions with Kr. We observe in Fig. 6 that this crossing will be accessible for thermal or hyperthermal collisions only for near-linear  $\text{KrOH}$  geometries (e.g.  $\theta = 170^\circ$  in Fig. 6). The extent of this mixing is governed by the strength of the coupling ( $V_{\Sigma\Pi}$ ) between the  $\Pi_{A'}$  and  $\Sigma_{A'}$  diabats.

**Trajectory Surface Hopping Calculations.** The quasiclassical trajectory (QCT) method employed in this work is similar to that described in previous papers,<sup>6,43</sup> and only those details relevant to the present work are included here. The non-adiabatic classical calculations were carried out by the Trajectory Surface Hopping (TSH) method<sup>44</sup> using the *fewest switches* algorithm proposed by Tully.<sup>45</sup> Trajectories are propagated classically on the electronically adiabatic  $1A'$  and  $2A'$  PESs. Trajectories were started on the upper PES. In the QCT-TSH method, the kinetic coupling between these two states is the product of the NACMEs [Eq. (4)]



and the nuclear velocities. As shown in Eq. (4), the NACMEs are derivatives of the diabatic mixing angles, which can be evaluated [Eqs. (2) and (3)] from the off-diagonal diabatic  $V_{\Sigma\Pi}$  PES and the adiabatic potentials. The evolution with the nuclear motion of the electronic population in the two states of A' reflection symmetry was controlled by integrating the time-dependent Liouville equation of the density matrix with a predictor-corrector Adams-Bashforth-Moulton algorithm, simultaneously to the trajectory propagation.

Fast variations of the electronic populations can cause trajectories to jump from the current electronic state to any other of the same symmetry. We found that a time step of 0.05 fs was sufficiently small to ensure the conservation of the trace of the density matrix – the total electronic population – as well as the total energy of the system. Batches of  $3 \times 10^5$  trajectories were run for each initial level at a collision energy of 39 meV. The initial distance between the incoming atom and the center of mass of the diatom was chosen to be 12 Å. The assignment of the final internal levels of the OH,  $N_f$ , were carried out by equating the classical rotational angular momentum to  $\hbar[N_f(N_f + 1)]^{1/2}$ . Real values of  $N_f$  are rounded to the nearest integer.

Also in order to conserve the total energy of the system after a transition to the other adiabatic PES's, a kinetic energy correction is performed by rescaling the momentum of each nucleus in the direction of the non-adiabatic coupling vector [Eq. (5)].<sup>45,46</sup> If the velocity component along the non-adiabatic coupling vector is not enough to overcome the energy gap, the jump is forbidden. In the strong interaction region (the region of the Kr–OH well) trajectories were found to undergo several hops (usually from 1 to 4) between the 1A' and 2A' PESs. An even number of switches results in an inelastic transition on the original PES. An odd number of jumps gives rise to a quenched trajectory from the excited 2A' to the ground 1A' state.

Figure 4 displays the comparison between the experimental and QCT-TSH rotational distribution of the nascent OH  $X^2\Pi$  formed by quenching from the lowest rotational level ( $N=0$ ) of the excited OH  $A^2\Sigma^+$  state with Kr as the collision partner. At a fixed collision energy of  $E_{\text{coll}} = 39$  meV, the total quenching cross section from the  $N=0$  level was found to be  $\sigma_Q(\text{TOT}) = 12.8 \text{ \AA}^2$ . As commented on above, the theoretical prediction agrees with the experimental rotational distribution fairly well.

We also carried out QCT-TSH calculations for other initial OH  $A^2\Sigma^+$  rotational levels,  $N = 0-14$ , always at a collision energy of 39 meV. The QCT-TSH total quenching cross-sections, summed over final levels, are compared with experiment in Fig. 2 (open circles). Note that these calculations do not include the electron spin. Hence, identical results are displayed for both OH fine-structure levels in both panels of the figure.

The calculations successfully capture the correct order of magnitude for the quenching cross-sections and the trend with increasing  $N$ , although the size of the quenching cross-section is somewhat underestimated, especially with increasing OH rotation. The present TSH calculations consider only transitions between the upper and lower  $A'$  states induced only by the mixing of the two dominant electron occupancies of these states. Specifically not included is Coriolis coupling between the nominally  $\Sigma$  and  $\Pi$  states. This will provide an additional pathway for collisional quenching of the  $2A'$  state. Since the magnitude of Coriolis coupling will depend on the OH rotational quantum number, it will lead to a selective increase in quenching for the higher rotational levels. If this effect were sufficiently large, it will bring the theoretical results into a better agreement with the experiment.

## DISCUSSION

Collisional electronic quenching of OH  $A^2\Sigma^+$  by Kr results in OH  $X^2\Pi$  products formed primarily in the lowest vibrational level with a substantial degree of rotational excitation and essentially no  $p\pi$  orbital alignment (or  $\Lambda$ -doublet propensity). Branching fraction measurements for specific OH  $X^2\Pi$  product states were used to scale the overall product state distribution, which then accounts for nearly all of the quenching events. These experimental observables can be understood in terms of the properties of the PES's, in particular the diabatic coupling and angular gradients in the vicinity of avoided crossing.

The minimal vibrational excitation is consistent with the small change in OH bond length between the ground and excited electronic states ( $r_e = 0.9697$  and  $1.0121$  Å, respectively). The degree of vibrational excitation (83% and 12% in  $v''=0$  and 1, respectively) agrees well with the square of the vibrational overlap between OH  $A$  ( $v=0$ ) and OH  $X$  ( $v''=0$ ) or ( $v''=1$ ) (Franck-Condon factors), based on which we would predict a relative OH  $X^2\Pi$  vibrational distribution of 90.5% in  $v''=0$  and 9.2% in  $v''=1$ . Since quenching of OH  $A^2\Sigma^+$  ( $v=0$ ) by Kr leads overwhelmingly to OH  $X$  ( $v'' = 0$ ) products, the approximation of a frozen OH distance, made here in our theoretical simulations, should be justified.

The same quenching process results in significant rotational excitation with an average rotational energy  $\langle E_{rot} \rangle = 4400$  cm<sup>-1</sup> and average rotational quantum number  $\langle N'' \rangle = 14$  in  $v''=0$ . The QCT calculations predict a similarly high degree of rotational excitation with  $\langle E_{rot} \rangle = 5300$  cm<sup>-1</sup> and  $\langle N'' \rangle = 18$ . The overall shape of the QCT product rotational distribution is quite similar to the experimental result and the same fitting function (sum of two Fisher-Tippet functions) has been used to guide the eye in Fig. 4. Based on this fit, the QCT distribution peaks at  $\sim 14$  quanta

of OH rotation, followed by a slight dip, and then has a secondary peak at  $\sim 21$  quanta of OH rotation. The physical origin of the slight dip could be due to different pathways from the region of nonadiabatic coupling, resulting in different torques being applied to the OH radical; however, this has not been explored in depth. The significant rotational excitation seen here in our experimental and QCT theoretical studies is a characteristic feature in nonreactive quenching of OH A  $^2\Sigma^+$  by many molecular collision partners.<sup>13-17,19</sup> Notwithstanding, only  $\sim 1/8$  of the available energy appears as rotation.

Features of the OH + Kr PES's provide insight into the mechanism for quenching and the origin of the degree of rotational excitation seen in the OH X  $^2\Pi$  product state distributions. As revealed by Fig. 7, at low collision energies the crossing between the  $V_\Sigma$  and  $V_\Pi$  potentials is only accessible for near linear Kr–OH configurations ( $\theta \geq 160^\circ$ ). A barrier on the excited state surface separates the OH–Kr and Kr–OH configurations and restricts access to the narrow Kr–OH well region where the ground and excited diabatic surfaces cross. The strong dependence of quenching on OH A  $^2\Sigma^+$  orientation, specifically favoring the O-side of OH pointing toward Kr, has been seen in theoretical studies involving several molecular partners, most notably the OH + H<sub>2</sub> and OH + N<sub>2</sub> systems.<sup>17,22</sup>

On the excited-state surface, an attractive interaction directs the approaching partners towards either the linear HO–Kr configuration, the global minimum, or toward the linear OH–Kr configuration, a local minimum. In the deeper HO–Kr well, a narrow angular region about linearity is intersected by the ground state surface at small  $R$ . The collision partners that access this narrow region are funneled down to the ground-state surface, where they experience a steep angular gradient away from linear geometry. The strong torque resulting from this gradient results in significant rotational excitation of the OH X  $^2\Pi$  products. Similar angular gradients on

the potentials have been identified previously in the OH + H<sub>2</sub> system and qualitatively linked to the degree of rotational excitation of the OH products.<sup>11,13-20,27-29</sup> On the other hand, the region of coupling between the ground and excited states is limited to near-linear geometry (Fig. 7), which sets a limit to the amount of rotational excitation. This would explain why only 1/8 of the total available energy appears as OH rotation.

The coupling between the surfaces also plays an important role in the quenching events. The size of the off-diagonal coupling in the quasi-diabatic basis, shown in Fig. 8, illustrates the strength of the mixing between the ground and excited A' states. The coupling vanishes in linear geometry, increases to a maximum near 120° at 3.1–3.2 a<sub>0</sub>, decreases in magnitude, and then changes sign in near perpendicular geometry. The region of the strongest coupling is not energetically accessible. Nevertheless, coupling occurs throughout the crossing region in the HO-Kr well region with greater strength for increasingly bent configurations, thereby favoring these geometries in quenching events.

The surface-hopping QCT calculations presented here include only two PES's, the ground and excited A' states. Agreement with experimental quenching cross-sections is reasonable, but the theory underestimates somewhat the true extent of electronic quenching. Possibly expanding the theoretical treatment to include the lowest A'' surface will increase the efficiency of quenching, leading to better agreement with experiment. In particular, the overall KrOH rotational motion will couple the excited  $\Sigma_{A'}$  PES to the  $\Pi_{A''}$  PES. Experimentally, quenched OH products are distributed equally over the two  $\Lambda$ -doublet components of each rotational level, which differs from previous studies with H<sub>2</sub> and N<sub>2</sub> collision partners where a strong  $\Pi(A')$   $\Lambda$ -doublet preference was observed. The  $\Lambda$ -doublet propensity arising from quenching has not yet been examined theoretically. This suggests that an accurate model of the

distribution of the OH(X) products among the fine-structure and  $\Lambda$ -doublet multiplets will require inclusion of both the  $\Pi_{A'}$  and  $\Pi_{A''}$  PESs.

## CONCLUSIONS

Experiment reveals that OH  $A^2\Sigma^+$  is efficiently quenched by collisions with Kr, leading to OH  $X^2\Pi$  products in  $v''=0$  and to a much lesser extent in  $v''=1$ . The minimal degree of vibrational excitation is consistent with the small change in OH bond length in its ground and excited states, with nearly diagonal Franck-Condon overlap. The quenched products exhibit a significant degree of rotational excitation. This is well predicted by quasi-classical trajectory calculations based on *ab initio* PESs.

We interpret the quenching in terms of crossings between these PESs. The calculated PES's associated with the two electronic states of  $A'$  reflection symmetry cross in linear KrOH geometry, but undergo strong coupling as the triatomic system bends. This coupling gives rise to efficient population transfer from OH  $A^2\Sigma^+$  ( $v=0, N=0$ ) to OH  $X^2\Pi$  ( $v'', N''$ ) products. The crossing region is accessible at thermal or hyperthermal energies due to the deep well in the OH  $A^2\Sigma^+$  – Kr PES. This well is shallower for the interaction of OH with the lighter noble gases. Thus, for interactions with the lighter noble gases, the  $A$  and  $X$  state crossing is inaccessible<sup>47</sup> and the efficiency of electronic quenching is much less.

Classical-trajectory, surface-hopping calculations which include the coupling between the two  $A'$  electronic states are able to account qualitatively for the electronic quenching cross sections and OH  $X^2\Pi$  level populations observed experimentally. However, a careful comparison with experiment suggests that couplings to the lowest  $A''$  PES might be important.

Similar quantum simulations of the electronic quenching are in progress, the results of which will be presented elsewhere.

## **ACKNOWLEDGEMENTS**

The research at the University of Pennsylvania was supported by the Office of Basic Energy Sciences of the Department of Energy. M.H.A. and P.J.D. acknowledge the support of the National Science Foundation through grant no. CHE-1213332. F.J.A. acknowledges the financial support by the Spanish Ministry of Education and Science under Grant Nos. CTQ2008-02578/BQU, CSD2009-00038, and CTQ2012-37404-C02. M.B. thanks the EPSRC (U.K.) for Programme Grant No. EP/G00224X/1, which funded part of this research.

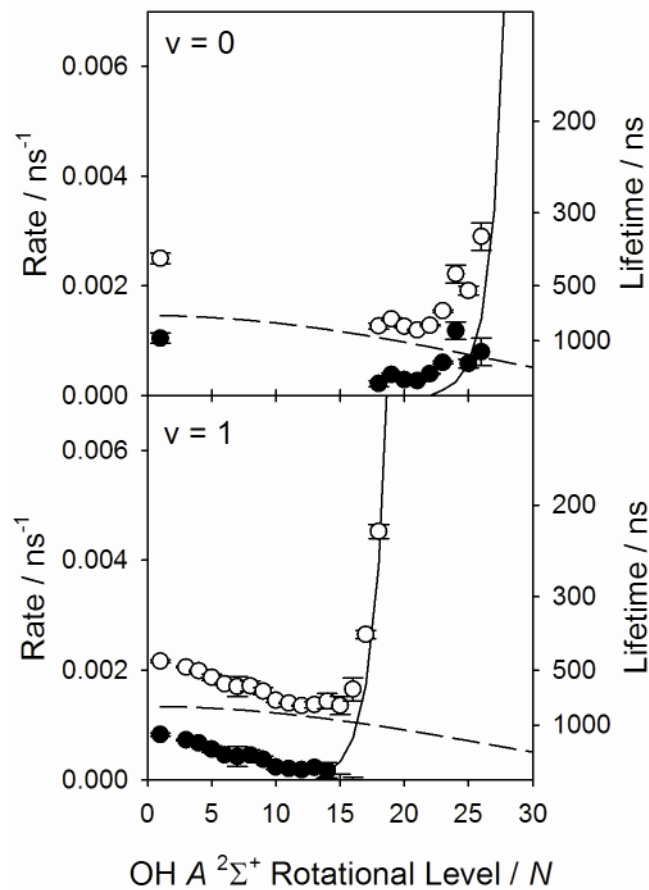


**Figure 1.** Experimentally determined OH A  $^2\Sigma^+$  total decay rates ( $k_{\text{tot}}$ ,  $\circ$ ) for  $v=0$  (top) and  $v=1$  (bottom) as a function of rotational level ( $N$ ) in the collisional region of the supersonic expansion (average collision energy of  $\sim 0.025$  eV). Pseudo first-order collisional rates ( $k_{\text{coll}}$ ,  $\bullet$ ) are derived from radiative ( $k_{\text{rad}}$ , dashed line) and predissociative ( $k_{\text{PD}}$ , solid line) rates from Ref. 37.



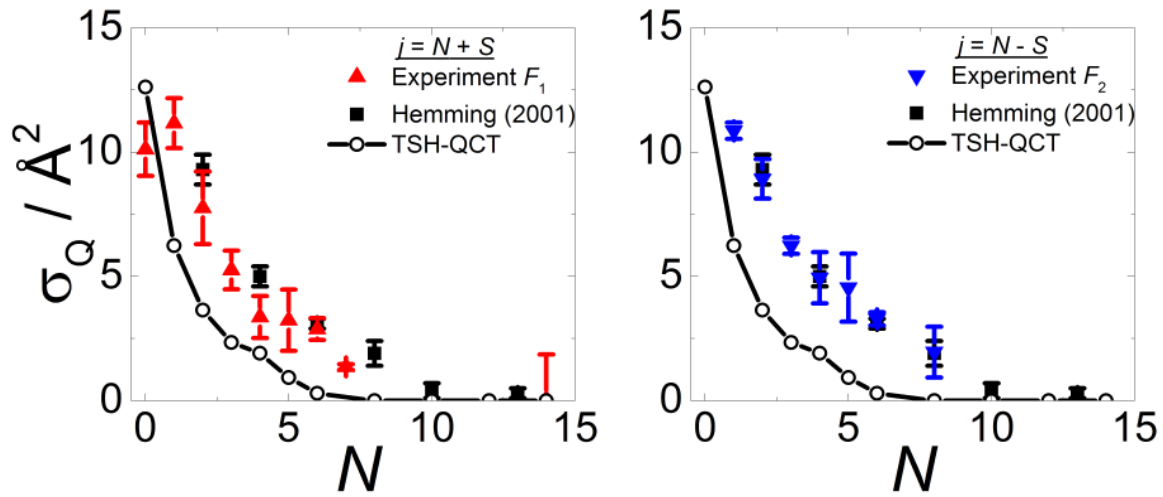


**Figure 2.** Electronic quenching cross-sections for OH  $A^2\Sigma^+$  ( $v=0$ ) with Kr under thermal conditions at 300 K. Left (red):  $F_1$ , right (blue):  $F_2$ , black squares: Hemming *et al.*<sup>5</sup> The open circles denote TSH-QCT closed-shell quenching cross-sections. Note that the spin-rotation level employed by Hemming *et al.* is not specified in their paper.

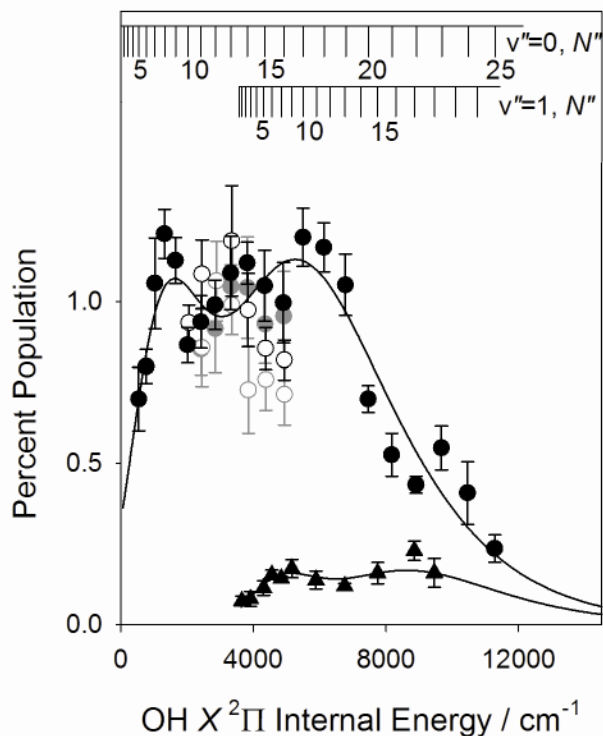


**Figure 3.** Nascent OH  $X^2\Pi$  quantum state distribution observed following quenching of OH  $A^2\Sigma^+$  ( $v=0, N=0$ ) by Kr as a function of OH  $X^2\Pi$  internal energy. Percent populations for  $v''=0$  (circles) and  $v''=1$  (triangles) are depicted. The  $F_1$  and  $F_2$  manifolds are shown in filled and open symbols, respectively, with black and grey symbols representing the  $\Pi(A')$  and  $\Pi(A'')$   $\Lambda$ -doublets, respectively. The fit through the data is primarily used as a guide to the eye, as described in the text.

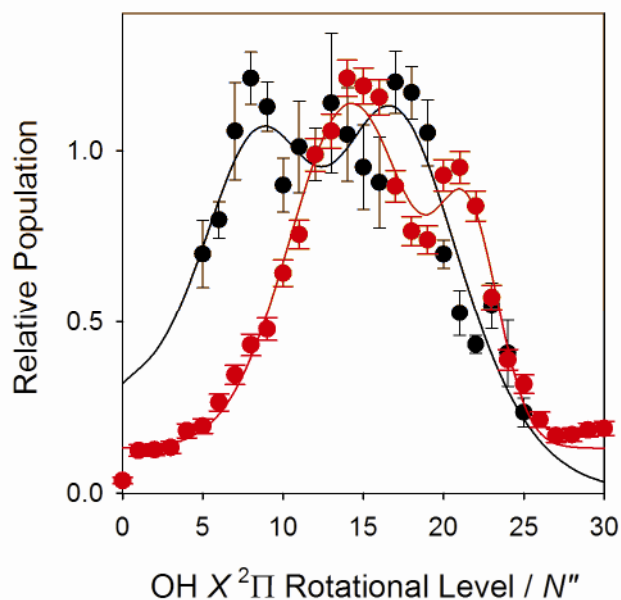


**Figure 4.** Nascent OH  $X^2\Pi$  quantum state distribution observed following quenching of OH  $A^2\Sigma^+$  ( $v=0$ ,  $N=0$ ) by Kr as a function of rotational level,  $N''$ . For simplification, the  $\Pi(A')$   $\Lambda$ -doublet for  $v''=0$  is depicted as an average of the  $F_1$  and  $F_2$  manifolds (black circles). The OH  $X^2\Pi$  rotational distribution resulting from QCT surface hopping calculations (red circles), arbitrarily scaled to the peak of the experimental distribution. The same functional form is used to fit both sets of data and is primarily used as a guide to the eye, as described in the text.

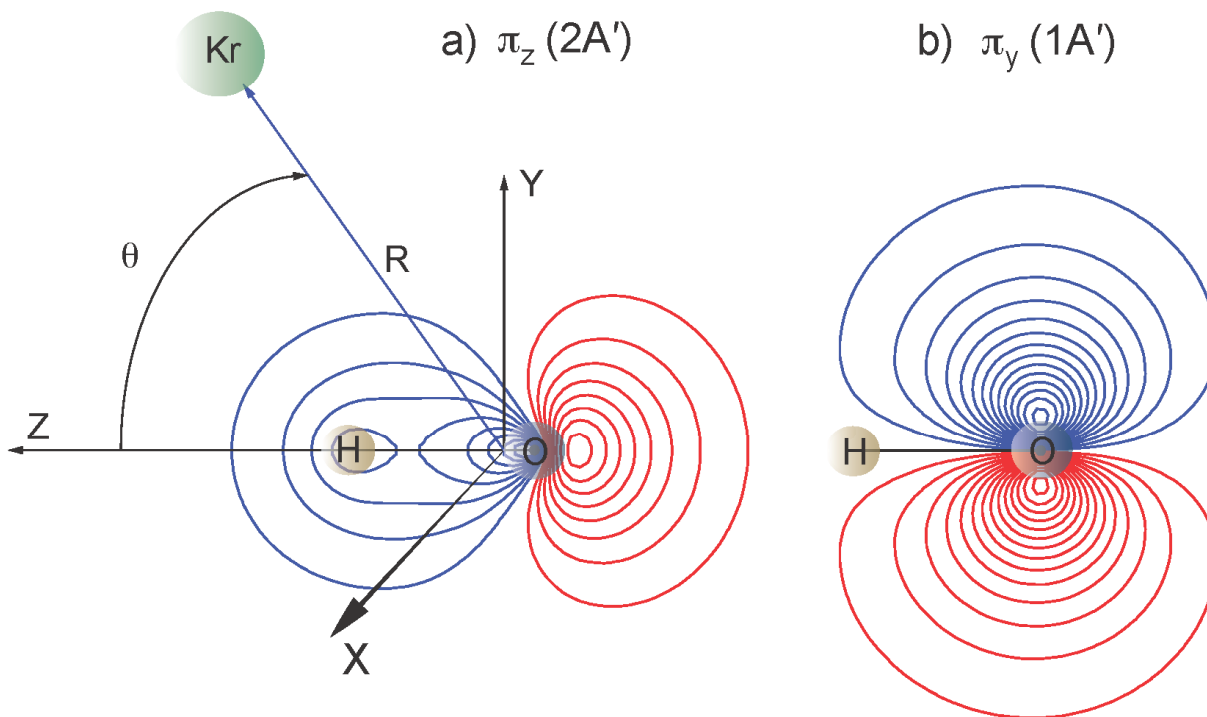


**Figure 5.** Visualization of the approach of the Kr atom (green sphere) to the (a) OH(A)  $\pi_z$  and (b) OH(X)  $\pi_y$  HOMO orbitals with shapes depicted qualitatively. The two orbitals are both symmetric ( $A'$ ) with respect to reflection in the triatomic plane.

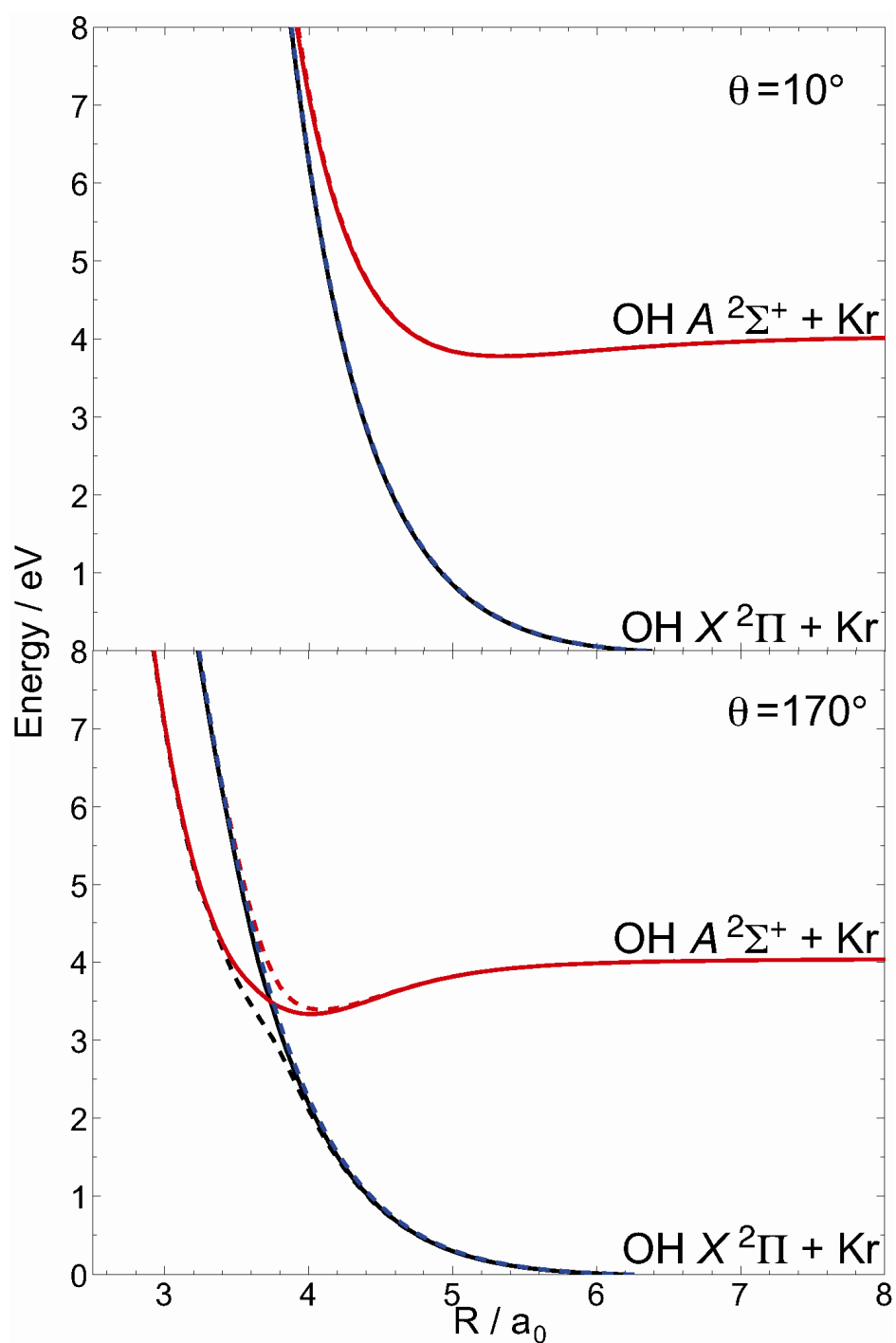


**Figure 6.** OH ( $X^2\Pi$ ,  $A^2\Sigma^+$ ) + Kr MRCISD+Q potential energy curves for the two states of  $A'$  reflection symmetry,  $\Pi_{A'}$  (solid black) and  $\Sigma_{A'}$  (solid red), as a function of the OH–Kr center-of-mass distance for near collinear OH–Kr (top panel) and HO–Kr (bottom panel) orientations. The black and red dashed lines indicate the  $1A'$  and  $2A'$  electronically adiabatic potential curves, and the blue dashed line is the  $1A''$  adiabatic potential curve.

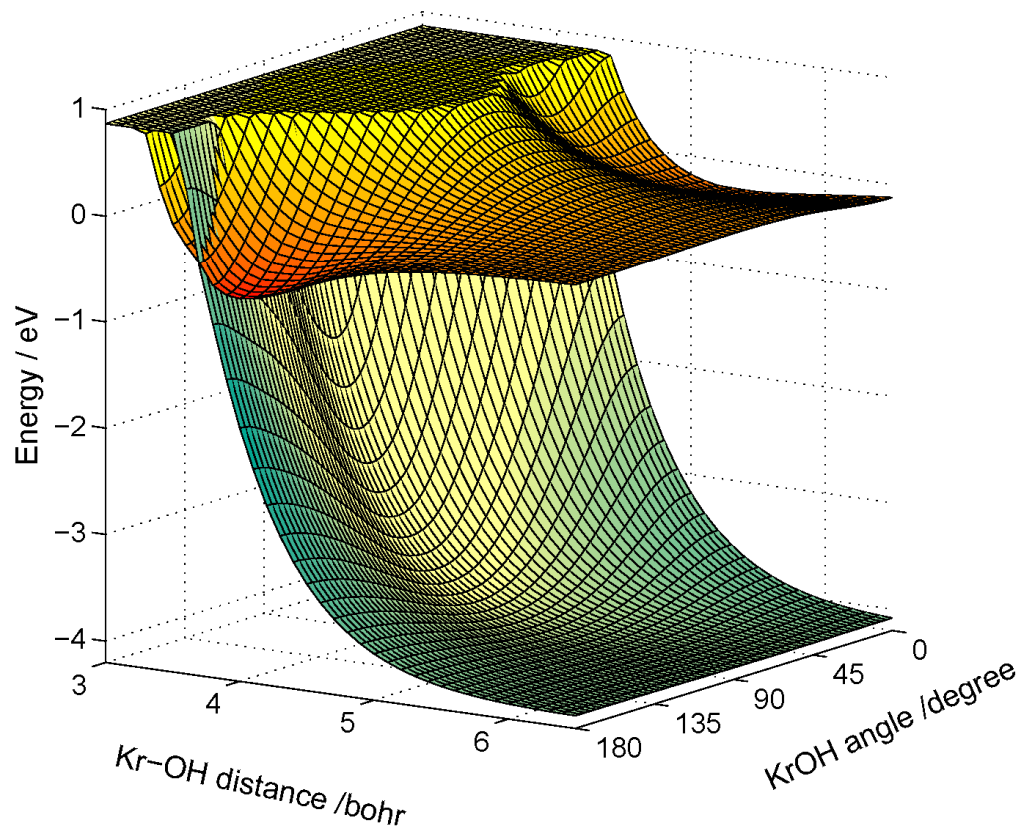


**Figure 7.** Surface plot relative to the OH  $A^2\Sigma^+ + \text{Kr}$  asymptote of the  $\Pi_{A'}$  (green) and  $\Sigma_{A'}$  (orange) diabatic states as a function of the OH to Kr center of mass distance ( $R$ ,  $a_0$ ) and the angle of OH with respect to Kr ( $\theta$ , degrees). The angular coordinate is defined in Fig. 5, where  $0^\circ$  and  $180^\circ$  correspond to linear OH–Kr and HO–Kr, respectively.

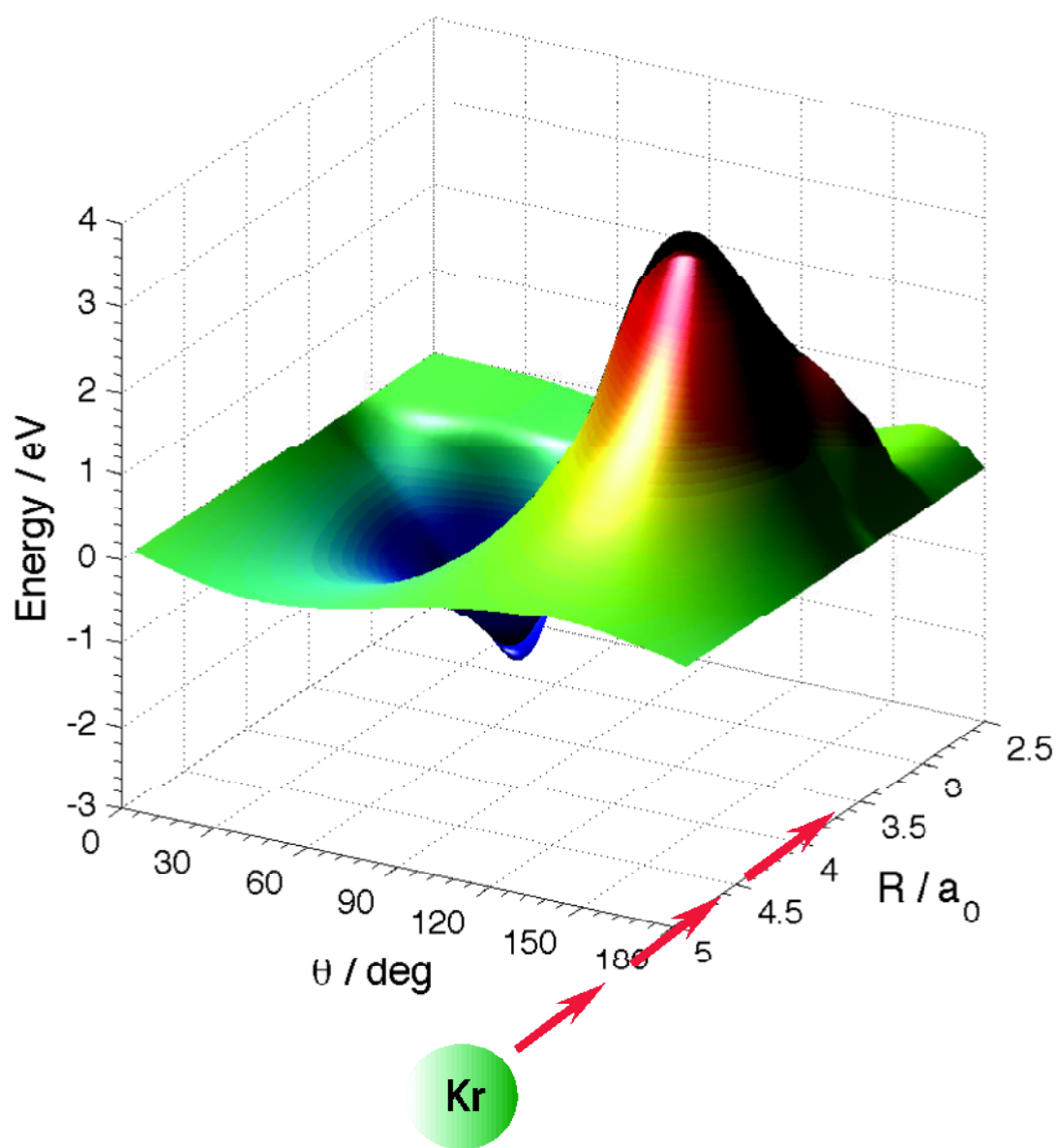


**Figure 8.** MRCISD+Q diabatic coupling  $V_{\Sigma\Pi}$  PES. The coupling vanishes in linear geometry and changes sign in near perpendicular geometry.

## REFERENCES

- (1) Crosley, D. R. Laser Fluorescence Detection of Atmospheric Hydroxyl Radicals. *Advanced Series in Physical Chemistry* **1995**, 3, 256-317.
- (2) Creasey, D. J.; Heard, D. E.; Pilling, M. J.; Whitaker, B. J.; Berzins, M.; Fairlie, R. Visualization of a Supersonic Free-Jet Expansion Using Laser-Induced Fluorescence Spectroscopy. Application to the Measurement of Rate Constants at Ultralow Temperatures. *Appl. Phys. B: Lasers Opt.* **1997**, 65, 375-391.
- (3) Heard, D. E.; Henderson, D. A. Quenching of  $\text{OH}(\text{A}^2\Sigma^+, v' = 0)$  by Several Collision Partners between 200 and 344 K. Cross-Section Measurements and Model Comparisons. *Phys. Chem. Chem. Phys.* **2000**, 2, 67-72.
- (4) Hemming, B. L.; Crosley, D. R. Rotational-Level Dependence of  $\text{OH A}^2\Sigma^+$  Quenching at 242 and 196 K. *J. Phys. Chem. A* **2002**, 106, 8992-8995.
- (5) Hemming, B. L.; Crosley, D. R.; Harrington, J. E.; Sick, V. Collisional Quenching of High Rotational Levels in  $\text{A}^2\Sigma^+$  OH. *J. Chem. Phys.* **2001**, 115, 3099-3104.
- (6) Chadwick, H.; Brouard, M.; Chang, Y. P.; Eyles, C. J.; Perkins, T.; Seamons, S. A.; Kłos, J.; Alexander, M. H.; Aoiz, F. J. A New Potential Energy Surface for  $\text{OH}(\text{A}^2\Sigma^+)$ -Kr: The van der Waals Complex and Inelastic Scattering. *J. Chem. Phys.* **2012**, 137, 154305.
- (7) Hogan, P.; Davis, D. D. Electronic Quenching and Vibrational Relaxation of the  $\text{OH}(\text{A}^2\Sigma^+, v'=1)$  State. *J. Chem. Phys.* **1975**, 62, 4574-4576.
- (8) Hogan, P.; Davis, D. D. Comments on "Electronic Quenching and Vibrational Relaxation of the  $\text{OH}(\text{A}^2\Sigma^+, v' = 1)$  state". *J. Chem. Phys.* **1976**, 64, 3901.
- (9) Lengel, R. K.; Crosley, D. R. Comment on "Electronic Quenching and Vibrational Relaxation of the  $\text{OH}(\text{A}^2\Sigma^+, v' = 1)$  State". *J. Chem. Phys.* **1976**, 64, 3900-3901.
- (10) Wysong, I. J.; Jeffries, J. B.; Crosley, D. R. Quenching of  $\text{A}^2\Sigma^+$  OH at 300K by Several Colliders. *J. Chem. Phys.* **1990**, 92, 5218-5222.
- (11) Ortiz-Suárez, M.; Witinski, M. F.; Davis, H. F. Reactive Quenching of  $\text{OH}(\text{A}^2\Sigma^+)$  by  $\text{D}_2$  Studied Using Crossed Molecular Beams. *J. Chem. Phys.* **2006**, 124, 201106.
- (12) Hancock, G., personal communication.
- (13) Cleary, P. A.; Dempsey, L. P.; Murray, C.; Lester, M. I.; Kłos, J.; Alexander, M. H. Electronic Quenching of  $\text{OH A}^2\Sigma^+$  Radicals in Single Collision Events with Molecular Hydrogen: Quantum State Distribution of the  $\text{OH X}^2\Pi$  Products. *J. Chem. Phys.* **2007**, 126, 204316.
- (14) Dempsey, L. P.; Murray, C.; Cleary, P. A.; Lester, M. I. Electronic Quenching of  $\text{OH A}^2\Sigma^+$  Radicals in Single Collision Events with  $\text{H}_2$  and  $\text{D}_2$ : A Comprehensive Quantum State Distribution of the  $\text{OH X}^2\Pi$  Products. *Phys. Chem. Chem. Phys.* **2008**, 10, 1424-1432.
- (15) Dempsey, L. P.; Murray, C.; Lester, M. I. Product Branching between Reactive and Non-Reactive Pathways in the Collisional Quenching of  $\text{OH A}^2\Sigma^+$  Radicals by  $\text{H}_2$ . *J. Chem. Phys.* **2007**, 127, 151101.
- (16) Dempsey, L. P.; Sechler, T. D.; Murray, C.; Lester, M. I. Quantum State Distribution of the  $\text{OH X}^2\Pi$  Products from Collisional Quenching of  $\text{OH A}^2\Sigma^+$  by  $\text{O}_2$  and  $\text{CO}_2$ . *J. Phys. Chem. A* **2009**, 113, 6851-6858.
- (17) Dempsey, L. P.; Sechler, T. D.; Murray, C.; Lester, M. I.; Matsika, S. State-Resolved Distribution of  $\text{OH X}^2\Pi$  Products Arising from Electronic Quenching of  $\text{OH A}^2\Sigma^+$  by  $\text{N}_2$ . *J. Chem. Phys.* **2009**, 130, 104307.



- (18) Lehman, J. H.; Bertrand, J. L.; Stephenson, T. A.; Lester, M. I. Reactive Quenching of OD  $A^2\Sigma^+$  by H<sub>2</sub>: Translational Energy Distributions for H- and D-Atom Product Channels. *J. Chem. Phys.* **2011**, *135*, 144303.
- (19) Lehman, J. H.; Dempsey, L. P.; Lester, M. I.; Fu, B.; Kamarchik, E.; Bowman, J. M. Collisional Quenching of OD  $A^2\Sigma^+$  by H<sub>2</sub>: Experimental and Theoretical studies of the State-Resolved OD  $X^2\Pi$  Product Distribution and Branching Fraction. *J. Chem. Phys.* **2010**, *133*, 164307.
- (20) Lehman, J. H.; Lester, M. I.; Yarkony, D. R. Reactive Quenching of OH  $A^2\Sigma^+$  by O<sub>2</sub> and CO: Experimental and Nonadiabatic Theoretical Studies of H- and O-Atom Product Channels. *J. Chem. Phys.* **2012**, *137*, 094312.
- (21) Alexander, M. H.; Andresen, P.; Bacis, R.; Bersohn, R.; Comes, F. J.; Dagdigian, P. J.; Dixon, R. N.; Field, R. W.; Flynn, G. W.; Gericke, K.-H., et al. A Nomenclature for  $\Lambda$ -Doublet Levels in Rotating Linear Molecules. *J. Chem. Phys.* **1988**, *89*, 1749-1753.
- (22) Hoffman, B. C.; Yarkony, D. R. The Role of Conical Intersections in the Nonadiabatic Quenching of OH( $A^2\Sigma^+$ ) by Molecular Hydrogen. *J. Chem. Phys.* **2000**, *113*, 10091-10099.
- (23) Lester, M. I.; Loomis, R. A.; Schwartz, R. L.; Walch, S. P. Electronic quenching of OH  $A^2\Sigma^+$  ( $v' = 0, 1$ ) in complexes with hydrogen and nitrogen. *J. Phys. Chem. A* **1997**, *101*, 9195-9206.
- (24) Yarkony, D. R. Current Issues in Nonadiabatic Chemistry. *J. Phys. Chem.* **1996**, *100*, 18612-18628.
- (25) Yarkony, D. R. Substituent Effects and the Noncrossing Rule: The Importance of Reduced Symmetry Subspaces. I. The Quenching of OH( $A^2\Sigma^+$ ) by H<sub>2</sub>. *J. Chem. Phys.* **1999**, *111*, 6661-6664.
- (26) Miller, S. M.; Clary, D. C.; Kliesch, A.; Werner, H. J. Rotationally Inelastic and Bound State Dynamics of H<sub>2</sub>-OH( $X^2\Pi$ ). *Mol. Phys.* **1994**, *83*, 405-428.
- (27) Bowman, J. M.; Czako, G.; Fu, B. High-dimensional Ab Initio Potential Energy Surfaces for Reaction Dynamics Calculations. *Phys. Chem. Chem. Phys.* **2011**, *13*, 8094-8111.
- (28) Fu, B.; Kamarchik, E.; Bowman, J. M. Quasiclassical Trajectory Study of the Postquenching Dynamics of OH  $A^2\Sigma^+$  by H<sub>2</sub>/D<sub>2</sub> on a Global Potential Energy Surface. *J. Chem. Phys.* **2010**, *133*, 164306.
- (29) Kamarchik, E.; Fu, B. N.; Bowman, J. M. Communication: Classical Trajectory Study of the Postquenching Dynamics of OH  $A^2\Sigma^+$  by H<sub>2</sub> Initiated at Conical Intersections. *J. Chem. Phys.* **2010**, *132*, 091102.
- (30) Zhang, P. Y.; Lu, R. F.; Chu, T. S.; Han, K. L. Nonadiabatic Quantum Reactive Scattering of the OH( $A^2\Sigma^+$ ) + D<sub>2</sub>. *J. Chem. Phys.* **2010**, *133*, 174316.
- (31) Zhang, P. Y.; Lu, R. F.; Chu, T. S.; Han, K. L. Quenching of OH( $A^2\Sigma^+$ ) by H<sub>2</sub> through Conical Intersections: Highly Excited Products in Nonreactive Channel. *J. Phys. Chem. A* **2010**, *114*, 6565-6568.
- (32) Carter, C. C.; Lee, H. S.; McCoy, A. B.; Miller, T. A. The Structure of Floppy Molecules: the Rg.XH/D (Rg = Ar, Ne, and Kr, X = O or S) Family of Complexes. *J. Molec. Struct.* **2000**, *525*, 1-45.
- (33) Carter, C. C.; Miller, T. A.; Lee, H. S.; Korambath, P. P.; McCoy, A. B.; Hayes, E. F. High Resolution Electronic Spectroscopy of Kr.OH/D and an Empirical Potential Energy Surface. *J. Chem. Phys.* **1999**, *110*, 1508-1520.
- (34) Fei, S. L.; Zheng, X. N.; Heaven, M. C. Electronic Spectroscopy and Vibrational Predissociation Dynamics of OH-Kr and OD-Kr. *J. Chem. Phys.* **1992**, *97*, 1655-1663.

- (35) Lemire, G. W.; Sausa, R. C. Detection and Spectroscopic Studies of Gas-Phase OH-Kr by Laser-Induced Fluorescence. *J. Phys. Chem.* **1992**, *96*, 4821-4824.
- (36) Brouard, M.; Bryant, A.; Chang, Y.-P.; Cireasa, R.; Eyles, C. J.; Green, A. M.; Marinakis, S.; Aoiz, F. J.; Kłos, J. Collisional Depolarization of OH(A) with Ar: Experiment and Theory. *J. Chem. Phys.* **2009**, *130*, 044306.
- (37) Luque, J.; Crosley, D. R. LIFBASE: Database and Spectral Simulation Program (Version 1.6). *SRI International Report MP 99-009* **1999**.
- (38) *Handbook of Mathematical Functions with Formulas, Graphs and Mathematical Tables*; Abramowitz, M.; Stegun, I., Eds.; Dover Publications: New York, 1972.
- (39) Alexander, M. H.; Corey, G. C. Collision-Induced Transitions between  $^2\Pi$  and  $^2\Sigma$  States of Diatomic Molecules - Quantum Theory and Collisional Propensity Rules. *J. Chem. Phys.* **1986**, *84*, 100-113.
- (40) Dagdigian, P. J.; Patel-Misra, D.; Berning, A.; Werner, H.-J.; Alexander, M. H. A Joint Experimental and Theoretical study of  $A^2\Pi - X^2\Sigma^+$  Electronic Energy Transfer in the CN Molecule Induced by Collisions with He. *J. Chem. Phys.* **1993**, *98*, 8580-8592.
- (41) Huber, K. P.; Herzberg, G. *Molecular Spectra and Molecular Structure. IV. Constants of Diatomic Molecules*; Van Nostrand Reinhold: New York, 1979.
- (42) Wilson, A. K.; Woon, D. E.; Peterson, K. A.; Dunning, T. H., Jr. Gaussian Basis Sets for Use in Correlated Molecular Calculations. IX. The Atoms Gallium through Krypton. *J. Chem. Phys.* **1999**, *110*, 7667-7676.
- (43) Aoiz, F. J.; Brouard, M.; Eyles, C. J.; Kłos, J.; de Miranda, M. P. The Collisional Depolarization of  $^{2S+1}\Sigma$  Radicals by Closed Shell Atoms: Theory and Application to OH( $A^2\Sigma^+$ ) + Ar. *J. Chem. Phys.* **2009**, *130*, 044305.
- (44) Tully, J. C.; Preston, R. K. Trajectory Surface Hopping Approach to Nonadiabatic Molecular Collisions: The Reaction of  $H^+$  with  $D_2$ . *J. Chem. Phys.* **1971**, *55*, 562-572.
- (45) Tully, J. C. Molecular Dynamics with Electronic Transitions. *J. Chem. Phys.* **1990**, *93*, 1061-1071.
- (46) Fabiano, E.; Keal, T. W.; Thiel, W. Implementation of Surface Hopping Molecular Dynamics using Semiempirical Methods. *Chem. Phys.* **2008**, *349*, 334-347.
- (47) J. Kłos, M. H. Alexander, P. J. Dagdigian, work in progress (2013).

Table of Contents graphic:

